7-1990

# Experimental Apparatus for Production, Cooling, and Storing Multiply Charged Ions for Charge-Transfer Measurements

Victor H. S. Kwong
*University of Nevada, Las Vegas*, victor.kwong@unlv.edu

T. T. Gibbons
*University of Nevada, Las Vegas*

Z. Fang
*University of Nevada, Las Vegas*

Jinhua Jiang
*Desert Research Institute*, Jinhua.Jiang@dri.edu

H. Knocke
*University of Nevada, Las Vegas*

# Experimental apparatus for production, cooling, and storing multiply charged ions for charge-transfer measurements

V. H. S. Kwong, T. T. Gibbons, Z. Fang, J. Jiang, H. Knocke, Y. Jiang, B. Ruger, S. Huang, E. Braganza, and W. Clark
*Department of Physics, University of Nevada, Las Vegas, 4505 Maryland Parkway, Las Vegas, Nevada 89154*

L. D. Gardner
*Harvard-Smithsonian Center for Astrophysics, 60 Garden Street, Cambridge, Massachusetts 02138*

(Received 27 November 1989; accepted for publication 22 March 1990)

A novel method is described that combines the production of ions by laser ablation with an ion-trap technique for the measurement of thermal-energy charge-transfer rates of multiply charged ions and neutrals. The charge-transfer rate is determined by measuring the rate of loss of stored ions from the trap. Verification of the calibration of the apparatus is demonstrated through investigation of charge transfer of $N_2$ and $N^{2+}$, which has been studied by another group. We also have made the first measurement on the thermal-energy charge-transfer coefficient of Ar and $W^{2+}$. The rate coefficient is $0.99(0.22)\times10^{-11}$ $cm^3\,s^{-1}$.

## I. INTRODUCTION

Measurement of thermal-energy charge-transfer processes involving multiply charged ions and neutral atoms is important for verifying the various theoretical treatments of the electron-capture processes.[1–3] It is of major importance to the understanding of interactions among the impurity ions and neutrals at the edges of tokamak fusion plasmas.[4,5] Knowledge of such charge-transfer rates also has considerable impact on studies relating to the generation of x-ray or vacuum ultraviolet (vuv) laser light.[6–9]

Two major approaches have traditionally been used in the study of charge-transfer collisions between multiply charged ions and neutrals: ion-beam technique[10–12] and the ion-trap approach.[13,14] The beam-target approach allows studies to be carried out at or above 0.1 keV/amu. Using the merged-beam technique,[15] the study has been extended to collision energies as low as 0.9 eV/amu. The ion-trap approach is known to accommodate energies well below 1 eV/amu. The primary weakness of this approach, however, lies in its ion source, which commonly utilizes electron-impact dissociative ionization of a molecular gas[13,16] or the electron-impact ionization of an atomic gas. The limited choice of a parent gas and small dissociative ionization cross section permits the production by this technique of only a very few types of singly or multiply charged ions in sufficient quantity for study.[17] Experiments are further complicated by the interaction of the ions with the parent source gas. Several approaches have been introduced to overcome the limitations. Vane, Prior, and Marrus[14] have used collisions between very energetic heavy ions (3.5 MeV/amu $Xe^{27+}$) and neon-gas atoms to produce and trap multiply charged neon recoil ions. Church *et al.*[18] have trapped near-room-temperature highly stripped ions of the noble gases following inner-shell excitation and subsequent decay by multiple electron emission (so-called "shake-off") induced by absorption of synchrontron radiation. An electron-beam ion trap (EBIT) has been built for the production of low-energy very highly charged ions and the study of their collisions with electrons.[19,20] However, these techniques are not well suited to the study of charge transfer between ions and neutral atoms and molecules other than the ions' parent gas, and no measurements have been carried out.

More recently, Kwong[21] has introduced a novel approach that combines the production of ions by laser ablation with the ion-trap technique. The energy of the ions ($W^{q+}$ with $1\leqslant q\leqslant 4$ and $Mo^{q+}$ with $1\leqslant q\leqslant 6$) stored in the trap has been estimated to be less than $4\times10^{-3}$ eV/amu. We will discuss the apparatus and technique in some detail. We will also present the first measurements of the thermal energy charge-transfer rate of Ar with $W^{2+}$. A detailed schematic of the apparatus is presented in Fig. 1.

## II. PRINCIPLE OF ION COOLING

Laser ablation has been used previously to produce both neutral atoms and ions[22–25] from solids. The number and charge states of ions produced by laser ablation depends on the laser energy and laser power density. The number of ions produced per laser shot is large, typically ranging from $10^{15}$ to $10^{17}$. The kinetic energy, however, is large (tens to hundreds of eV). It is essential that the kinetic energies of multiply charged ions from ablation plasmas be substantially reduced, if they are to be captured in the relatively shallow potential well (a few eV) of a typical ion trap. The cooling of laser-ablated ions can be achieved by using two separate beams which cross at right angles inside the ion trap. A few ions in one beam undergo collisions with ions from the other beam with the result that some of the scattered ions lose almost all their kinetic energy (and remain inside the trap), while others approximately double theirs (and leave the trap). A simple classical analog of this cooling effect is the elastic collision of two billiard balls of identical mass $M$ and speeds $v_1$ and $v_2$ which approach one another along exactly orthogonal trajectories, say, from infinity along the $x$ and $y$ axes. When

 0034-6748/90/071931-09$02.00  

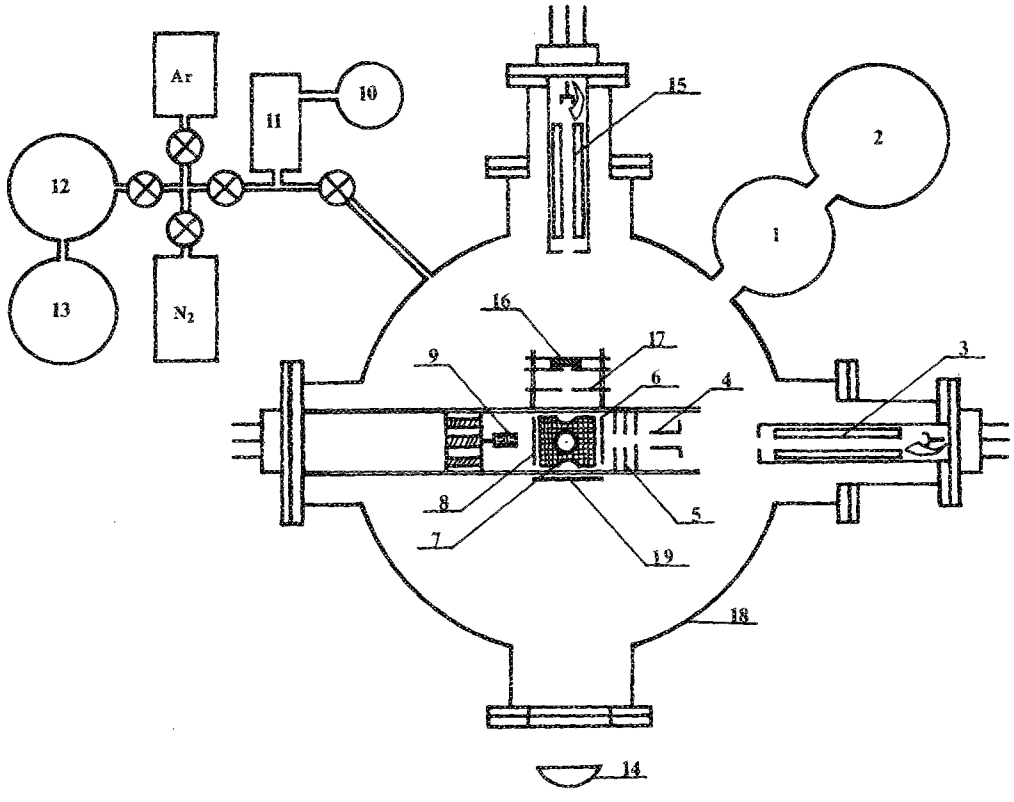


FIG. 1. Schematic view of the experimental apparatus. 1: 4-in. diffusion pump; 2: roughing pump; 3: Vacuum General Masstorr DX200 quadrupole mass analyzer; 4: deflection plates; 5: electrostatic lens; 6: ion-trap end-cap electrode No. 2; 7: ion-trap ring electrode; 8: ion-trap end-cap electrode No. 1; 9: electron gun; 10: Baratron-type 122A capacitance manometer; 11: gas reservoir; 12: liquid-nitrogen cold trap; 13: roughing pump; 14: quartz focusing lens; 15: Vacuum General Masstorr DX100 residual gas analyzer; 16: tungsten carbide target and mount; 17: beam skimmer; 18: ultrahigh-vacuum chamber; 19: Langmuir probe.

the line joining the centers of the billiard balls during impact is parallel to either one of the two initial trajectories, it is trivial to show, using conservation of energy and momentum, that after a perfectly elastic collision, one ball remains at the origin with zero velocity, and the other moves away along a line in the $x$-$y$ plane with a speed $v_r = (v_1^2 + v_2^2)^{1/2}$. In the case of collisions of multiply charged ions from the crossed abalation beams, only a small fraction of the number of collisions will result in ions which remain in the trap. Since there are $10^{15}$ or more ions in each abalation pulse, a small fraction is still a very large number. In practice, the number of ions that can be stored is limited to about $10^6$ because of space-charge effects.

## III. PROCEDURE FOR THE DETERMINATION OF CHARGE-TRANSFER RATES

Charge-transfer rates are determined by measuring the relative number of ions remaining in the trap as a function of the time $t_i$ after their production and of the pressure of the gas of interest. The ion trap is flooded with the gas of interest to a known pressure. The density of the gas is kept low enough that laser-induced gas breakdown does not occur along the path of the laser beam. The number of multiply charged ions present in the trap is determined by extracting them from the trap and detecting them with a channel electron multiplier (CEM). The temporal profile of the ion-signal amplitude is recorded by a transient digitizer, and the digitized signal is then stored in a computer for subsequent data analysis.

The charge-transfer rate is quite dependent on the energy states of the multiply charged ions. After laser ablation, substantial numbers of ions can be in various metastable states. For sufficiently short lifetimes of these metastable states, measurement can be made after the ions have decayed to their ground state. For longer lifetimes a multiexponential fit can be used.

In a situation where the ions are in the ground state, the resulting decay curve can be described by a simple exponential function:

$$N = N_0 e^{-Ct}, \text{ with } C = n\langle Qv\rangle + n'\langle Q'v\rangle,$$

where $N_0$ and $N$ are number of stored ions at time zero and time $t$, respectively. $\langle Qv\rangle$ and $\langle Q'v\rangle$ are the charge-transfer rate coefficient for the neutral gas and residual background of the vacuum system. $Q$ is the charge-transfer cross section, and $v$ is the relative velocity between ions and neutral atoms. $n$ and $n'$ are the particle density of neutral gas and residual background gas. The decay constant $C$ for each neutral gas can be extracted from the data by a least-squares fit to the time-dependent ion signal. Several decay constants $C$ were obtained for different neutral-gas densities. The charge-transfer rate coefficient for the neutral gas is determined from the slope of the decay constant $C$ vs $n$ curves. The intercept gives the value of $n'\langle Q'v\rangle$, the charge-transfer rate of multiply charged ions with the residual background gas. The values of $n$ and $n'$ can be accurately determined using a calibrated ion gauge and/or a residual gas analyzer.

## IV. LASER ABLATION ION SOURCE

A simplified schematic for the laser ablation ion source is given in Fig. 2. Two pieces of tungsten carbide attached to a stainless-steel mount are used as targets for the generation of tungsten ions. A stainless-steel skimmer with a

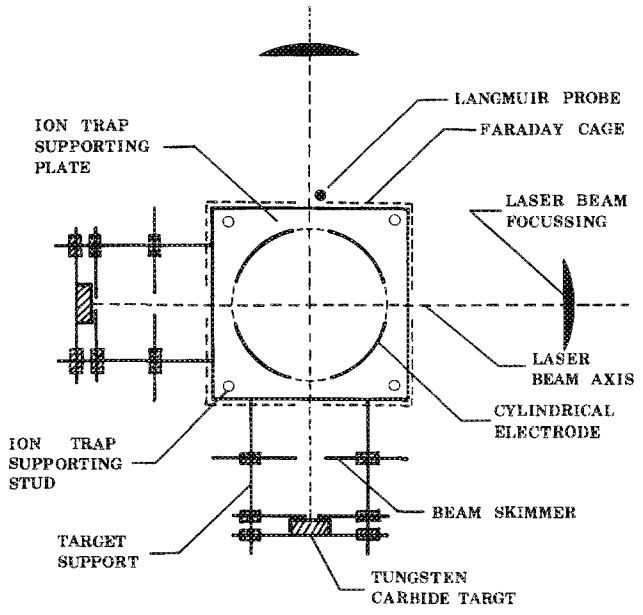


FIG. 2. Schematic of crossed-beams ion cooling system. This scheme is used to cool the energetic tungsten ions well below the trapping potential of the rf ion trap.

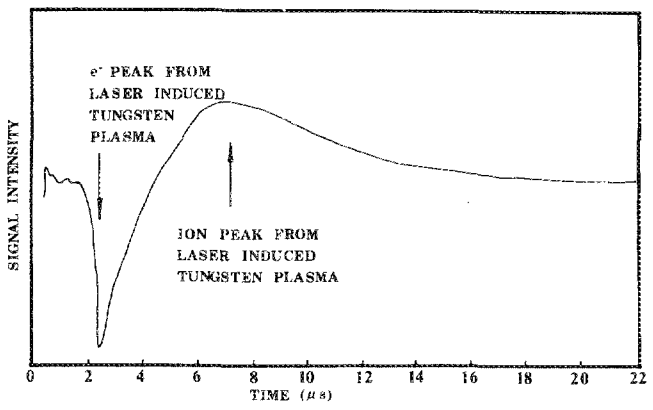


FIG 3. Bipolar signal obtained by a Langmuir probe mounted at a short distance away from the ion trap to monitor the energy of laser-induced tungsten ions.

4-mm-diam hole cut out at the center is positioned between each target and the ion trap, and used to collimate two expanding ion clouds from the laser-induced plasmas into two narrow cones. The ions stream into the trap through 5-mm-diam holes cut out of the ring electrode. The holes also permit the unobstructed passage of the ablation laser beam through the ion trap. Each target assembly (tungsten carbide target, target mounting plate, and skimmer) is held in position in the plane of the ring electrode and at the same fixed distance from its center by two stainless-steel studs attached to the ion-trap support structures. The arrangement minimizes the scattering of ions from the wall of the trap's ring electrode as they expand into and pass through the ion trap. The laser axes, perpendicular to the surface of each target, intersect at right angles at the center of the trap. The positioning of the two target assembles ensures the crossed-beam collisional configuration necessary for the cooling of energetic multiply charged ions from the laser ablation plasmas.

The two laser beams needed to simultaneously generate the ablation beams are obtained by splitting the output of the second harmonic of a Nd:YAG laser (Molectron MY-32 oscillator/amplifier system) using a 50:50 dielectric-coated beam splitter. The two pulsed laser beams are collimated so that they pass through the holes in the ring electrode and strike the targets unscattered. Each ablation beam is focused by a 25-cm-focal-length convex lens positioned outside the vacuum chamber. Fine focusing of each laser beam on the target surface is achieved by translating the lens along the laser axis until plasma formation is observed. Plasma formation can be detected by eye using a notch filter that blocks scattered light at the laser wavelength or electronically by the sudden deflection of an ion gauge. Each laser pulse has a measured energy of about 20 mJ, time duration of 25 ns, FWHM, and a spot size at the ablation target of 0.1 mm. The mean power density of the ablation laser at the target surface is estimated to be $1.2\times10^9$ W/cm$^2$.

The kinetic energy of the laser-induced ions is measured by a Langmuir probe installed 2 mm away from the ring electrode and positioned so as to collect some of the charged particles from one of the ablation beams (see Fig. 2). The current picked up by the probe provides time-of-flight information on the components of laser-induced plasmas. The position of the Langmuir probe near the ring electrode also allows it to be used as an antenna for the purpose of monitoring the amplitude and frequency of the rf applied to the trap's ring electrode.

Figure 3 shows a typical temporal profile of a laser-induced plasma as it passes through the ion trap and is picked up by the Langmuir probe. The signal is obtained by feeding the output of the Langmuir probe directly to a Tektronix 2235 oscilloscope. The negative-going portion of the pulse shown in Fig. 3 is mainly due to electron pickup by the probe, while the positive signal is due to ion pickup. The Langmuir probe cannot differentiate various charge states of the ions. The bipolar signal clearly indicates separation of charges in the laser-induced plasma. Electrons, being lighter in mass, have a higher expansion velocity and expand into the vacuum ahead of the heavier and slower moving ions. The spatial separation of these two groups of charged particles generates an electric field that decelerates the expansion of electrons while it accelerates the ions. Based on the time-of-flight information of the ion peak in Fig. 3, the mean energy of a laser-induced tungsten plasma ion is in excess of 250 eV. Their energies are far larger than the trapping potential of the trap.

The reproducibility, laser pulse to pulse, of the ion density in the trap is vitally important to the charge-transfer measurement. Figure 4 is a plot of ion signals as a function of the number of laser shots. The signal is obtained by dumping the ions from the ion trap to CEM after the ions are produced by laser ablation, collisionally cooled, and stored. It is clear that the ion signal is very reproducible over at least 80 shots. There is, however, a gradual decrease in ion signal due to the changing in laser

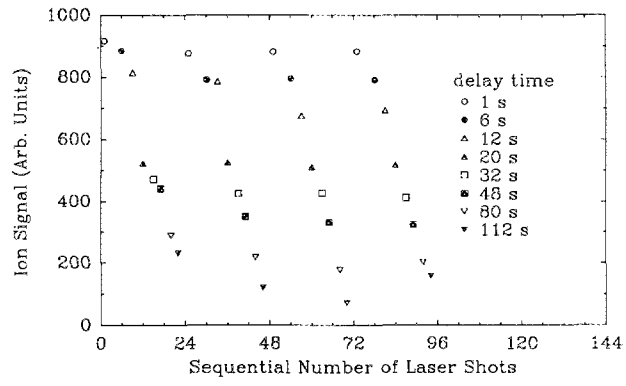


FIG. 4. Reproducibility of ion-signal intensity over the sequential number of laser shots. The delay time is determined by the initiation of the laser shot and the dumping of the stored ions into the CEM.

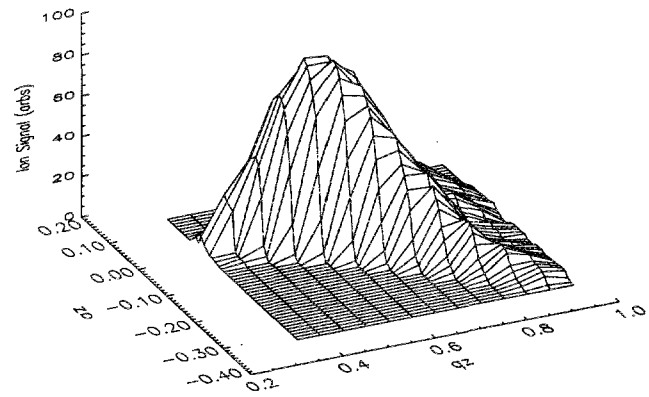


FIG. 5. A three-dimensional plot of $N_2^+$ signal as function of the Mathieu parameters $a_z$ and $q_z$. It shows the optimal storage region of $N_2^+$. $a_z$ and $q_z$ are related to $V_0$, $U_0$, and $\Omega_0$ discussed in the paper.

power density at the target surface as the target is gradually vaporized away. The reproducibility of the ion signals over 80 shots may be due to the huge disparity between number of ions produced by laser ablation and the relatively small number of ions that can actually be stored. Since the ion trap is filled each time, any change in the number density of ions produced by laser ablation due to fluctuation in the laser power is damped out. For all measurements, each ion-density decay curve was obtained with 100 or fewer laser shots. Systematic error due to gradual change in the power density of the laser is thereby eliminated.

## V. ION-TRAP ASSEMBLY AND THE VACUUM SYSTEM

The key component of the apparatus is the ion trap. It provides a relatively weak field (50 V/cm) to confine the ions. The ion trap used in our current system is a radio-frequency trap with a cylinderical ring electrode and two flat end caps. This design was chosen because of its simplicity in fabrication. The potential surfaces near the center of the trap approximate those produced by ideal hyperbolic electrodes. The stable trajectories of the stored ions in a periodic hyperbolic potential can be obtained from the solution of Mathieu equation.[26] The two parameters $q_z$ and $a_z$ determine the ion trajectories and are related to the ion charge state $q$, mass $M$, the trap's radius $r$, trap's length $2z_0$, rf frequency $\Omega_0$, rf amplitude $V_0$, and dc bias $U_0$, on the ring electrode by the following relations:

$$q_z = 8qV_0/3m(r_0\Omega_0)^2,$$

$$a_z = -[16qU_0/3m(r_0\Omega_0)^2],$$

with $r_0 = z_0$. The pseudopotential well depths in the axial and radial directions are given by

$$V_z = \left(\frac{4qV_0^2}{3m(r_0\Omega_0)^2} - \frac{2U_0}{3r_0^2}\right) r_0^2,$$

$$V_r = \left(\frac{qV_0^2}{3m(r_0\Omega_0)^2} + \frac{U_0}{3r_0^2}\right) r_0^2.$$

For a spherical pseudopotential well $V_s$, i.e., $V_z = V_r = V_s$, the well depth is given by

$$V_s = \tfrac{2}{3}(qV_0^2/m\Omega_0^2).$$

The storage characteristics of the rf cylindrical trap have been tested using $N^{2+}$, $N^+$, $Ar^{2+}$, and $Ar^+$ produced by electron-impact ionization of their parent gases. The regions of stability observed were found to be consistent with those calculated for a trap with hyperbolic electrodes. No noticeable shifting of the stable regions was observed.[21] The optimal ion-density region is between 0.55 and 0.60 along the spherical well line (see Fig. 5). We have therefore used the stability diagram for an ideal hyperbolic electrode trap to guide us in ion selection. Figure 5 is a three-dimensional plot of the ion density as a function of $a_z$ and $q_z$ inside the stable region.

The rf trap is made up of a cylinder (ring electrode) of radius 1.67 cm and length 3.34 cm with two flat end caps 3.40 cm in diameter. Both the ring electrode and end caps are fabricated from 30-gauge 304 stainless-steel mesh. Four 5-mm-diam holes are cut out in the ring electrode to allow for clear passage of the Nd:YAG laser beams through the trap. Stainless-steel mesh was used because of its strength in maintaining a rigid structure. In addition, the high transmission of the electrodes allows unwanted gas to escape the trap thus minimizing the backscattering of the laser-induced ions and equilibrating with the surrounding vaccum. The latter feature is of particular importance for the accurate determination of the density of gas such as $N_2$ or Ar admitted for charge-transfer measurements.

An electron gun is mounted outside the trap next to one of the end caps. It is primarily used to generate ions from atomic and molecular gases. Ions so produced are used to test the operation of the trap, to verify the trap characteristics, and to calibrate the system using an ion-neutral pair of known charge-transfer rate. The electron gun is not used when the laser ablation ion source is used.

A pair of deflection plates are mounted between the second end cap and the mass analyzer (quadrupole mass analyzer or a time-of-flight analyzer) with its detector. Potentials are applied to the plates when the electron gun or

the laser is on to prevent ions from reaching the detector and causing permanent damage. The whole ion trap is enclosed in a grounded Faraday cage made out of 10-gauge stainless-steel mesh, which minimizes the interference of the rf field on the expansion of the laser-induced ions as they drift towards the trap's ring electrode (see Fig. 2).

The trap assembly and mass analyzer/detector are housed inside a six-port stainless-steel ultrahigh-vacuum chamber sealed by 20-cm conflat flanges. The vacuum chamber is pumped by a diffusion pump (Varian VHS-4) with a liquid-nitrogen cold trap to optimize the pumping speed and minimize back streaming of oils from the diffusion pump (Dow-Corning 705) and the forepump. A residual background pressure of $1\times10^{-9}$ Torr (mainly water and molecular hydrogen) is routinely reached without baking. Background pressures of at least a factor of 10 lower can be achieved after baking the system. No baking was carried out in this series of experiments. The ion-trap ensemble is rigidly supported by four 5-mm threaded rods that attach firmly to a 20-cm stainless-steel conflat flange.

The two laser beams enter the chamber through Pyrex viewports. The control signals that operate the trap (including the rf voltage, electron gun bias, etc.) and those for the mass analyzer/detector enter the vacuum chamber through two separate UHV feedthroughs to minimize the rf and switching noise pickup. All cables that deliver control pulses to the ion trap inside the vacuum chamber are enclosed inside a Faraday cage to minimize stray rf field pickup by the signal cable.

During laser ablation, a significant quantity of gas is released in addition to the tungsten atoms and ions. Measurements using a nude ionization gauge indicated that the pressure inside the vacuum chamber rose momentarily to $10^{-5}$ Torr in the first initial laser shots. These initial bursts of gas during laser ablation was due to photo and thermal desorption of adsorbed gas on the target surface. However, the pressure rise diminishes to less than $10^{-8}$ Torr after 10–20 shots. Measurements were made after the target surface was cleaned by laser ablation. The pumping speed of the diffusion pump/cold trap combination was capable of reducing the background pressure to $10^{-9}$ Torr in less than 200 ms. Systematic effects associated with gas released from laser ablation of target are expected to be insignificant during the charge-transfer measurement.

## VI. TIMING ELECTRONICS

The proper operation of the apparatus requires that a number of signals of both polarities and varying amplitudes and pulse widths be applied in a well-defined sequence to a number of electrodes and to data-acquistion instruments. The appropriate signals are controlled by a central logic unit consisting of an LM555 oscillator, which provides the basic clock pulses, and several TTL monostable vibrators, AND gates, OR gates, and line buffers/drivers. The outputs of the logic circuits are coupled using optoisolators to high-voltage transistor switching circuits which produce pulses whose amplitudes range from 20 to 500 V and can be of either polarity.

The timing diagram is outlined in Fig. 6. The ion dump

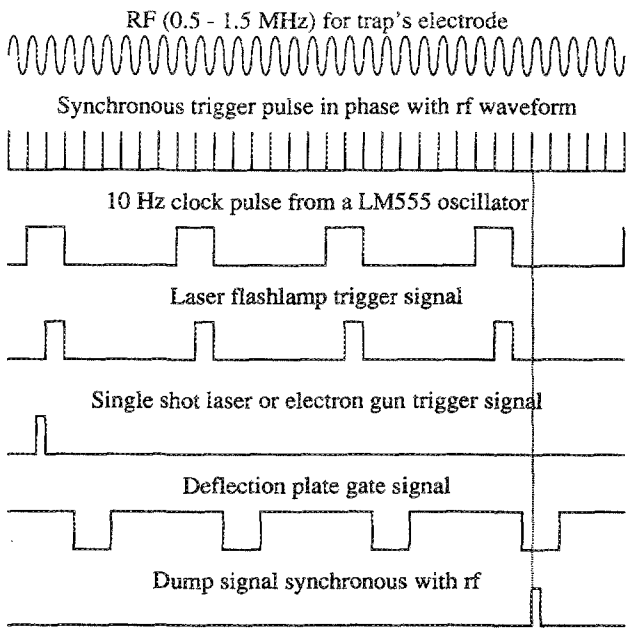


FIG. 6. Timing diagram for laser and ion trap.

pulses are synchronized to a specific phase of the rf waveform in order to minimize fluctuations in the number of ions ejected from the trap. The delay time between creation in ions and their ejection from the trap was monitored by a scope.

The Nd:YAG laser flashlamp and $Q$ switch were individually triggered by separately generated trigger pulses from the central timing unit. The flashlamp of the laser is pulsed at 10 Hz to achieve maximum stability of the laser output. The $Q$ switch, which actually initiates laser light emission, was pulsed in phase with the flashlamp, but at a much lower rate appropriate to the particular decay time under study. The period between two laser pulses ranged from few milliseconds to several seconds and was longer than the time duration for a measurement.

During the calibration experiments, measurements were made using ions created by electron bombardment on a gas admitted into the trap. The control pulse that normally initiated the signal shot firing of the laser was applied to high-voltage switching circuit connected to the electron-gun cathode. Electrons were thereby pulsed into the ion trap where they ionized some of the gas atoms and molecules present. The system was designed so that a wide range of ions could be produced.

Prior to the creation of ions, a gate pulse of $+100$ V was applied to one of the deflection plates between the trap and ion detector for about 5 ms to prevent any stray ions or electrons from entering the channel electron multiplier when the electron gun or laser was on.

## VII. ION TRANSPORT AND DETECTION

Ions stored in the trap are extracted from the trap by applying a 1.1-$\mu$s, $-70$-V negative-bias pulse with a rise time of 0.2 $\mu$s to the end cap facing the detector. Two modes of mass analysis/detection have been performed.

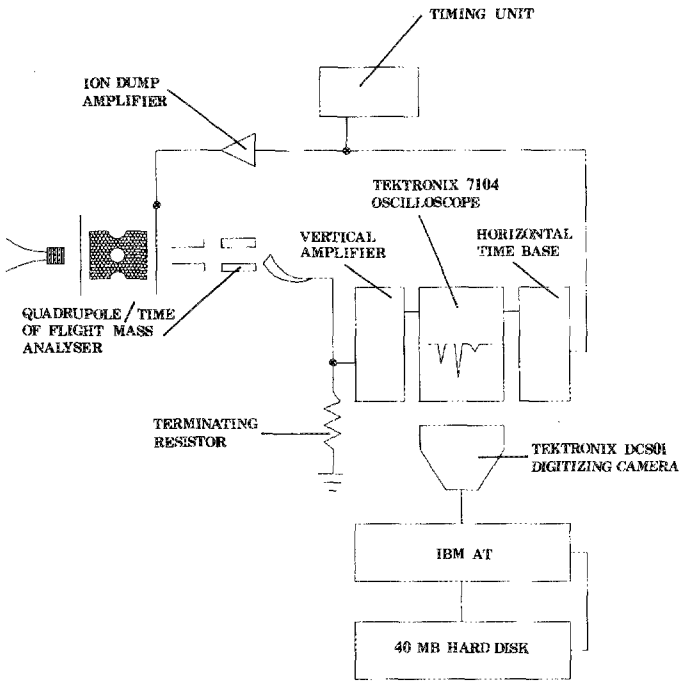


FIG. 7. Data-acquisition system used in charge-transfer experiment.

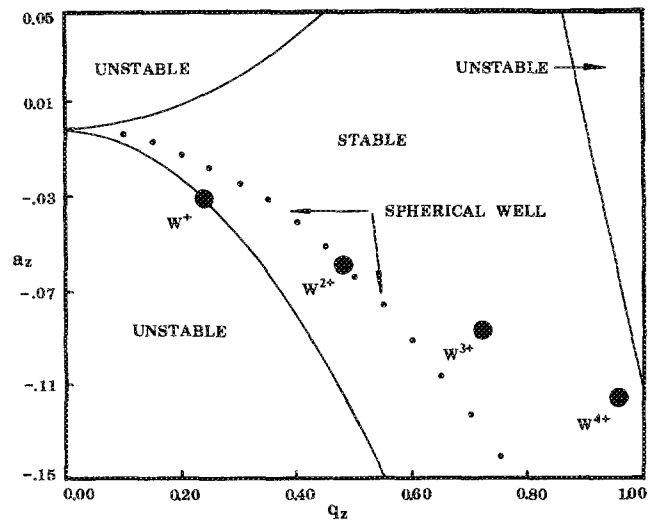


FIG. 8. $W^{q+}$ stability diagram. The ion trap is operated at the following parameters: $V_0 = 400$ V, $U_0 = 24$ V, and $f = 0.475$ MHz. Ions in the region labeled "stable" can be stored in the trap. The dc bias, $U_0$ on the ring electrode selects which ions are stored.

Initially, only a channel electron multiplier (Galileo model No. 4816) was used. Mass identification was made by the ion's time of flight. Additional mass identification was made with the aid of the trap's stability diagram and adjusting trap parameters to shift particular charge states close to the edges of the stable region. Mass identification was further confirmed by a Vacuum General Masstorr DX 200 quadrupole mass analyzer. The time-of-flight spectrum and the ions' mass-to-charge ratio provided by the quadrupole mass filter are in agreement with the picture of the trap's behavior based on its stability diagram. All the data used in our final analysis were obtained with a CEM TOF detector.

During the course of the experiment, it was also found out that the 1.1-$\mu$s bias on the lower second end cap was not adequate to extract all ions stored in the trap. The length of the bias pulse was increased to 2.6 $\mu$s, and the ion signal intensity increased several fold. The effective extraction potential seen by the ions is about 32 V and is due to a combination of the instantaneous rf potential, the dc bias on the ring electrode, and the negative extraction bias on the end cap at the time of ion ejection. Higher extraction potentials were not used in order not to exceed energies appropriate for the quadrupole mass filter to function effectively.

## VIII. DATA-ACQUISTION AND ANALYSIS SYSTEM

Figure 7 shows the block diagram for the data-acquistion system. Ions are detected by pulsing the ions from the ion trap into a CEM operated within the linear range. To ensure the linear response of the CEM the maximum peak current from the CEM is kept less than 10% of the CEM dc-bias current. Furthermore, the linearity region of the CEM is checked by plotting the CEM peak output current as a function of bias voltage for different ion intensities created by the electron gun. The region of linearity is reflected by the convergence of their slopes. We operated well below the saturation region.

The output from the anode of the CEM is directly fed to the 7A26 vertical amplifier in a Tektronix 7104 oscilloscope of 2-GHz bandwidth. The time sweep is initiated by the leading edge of the ion dump pulse. Since all ions pulsed out of the trap see the same extraction potential, the time of flight (TOF) of the ion is a function of the mass-to-charge ratio ($m/q$). The TOF spectrum is digitized by DCS-01 Tektronix digitizing camera system. The spectrum is fed directly into an IBM AT computer for storage and data analysis.

Five to ten measurements of the ion peak were made for a specific delay time. The individual measurements were averaged and stored in the computer's memory. Measurements were then repeated with different delay time. After accumulating data from several runs, the stored information was transferred to the computer's hard disk for archival and future analysis. Depending on the decay rate being measured, a complete set of data points for one decay curve could be obtained in a few minutes to half an hour. A multiexponential fitting routine was used to fit the time-dependent ion signal and extract the decay rates.

## IX. VERIFICATION OF EXPERIMENTAL PERFORMANCE

### A. Charge-state identification of ions

The charge states of ions produced by laser ablation are dependent on the power density of the ablation laser. Specific groups of ions can be stored in the trap by judicious choice of trapping parameters ($V_0$, $U_0$, $\Omega_0$). Figure 8 shows the theoretical stability diagram for tungsten ions obtained from the solution of the Mathieu equation for the

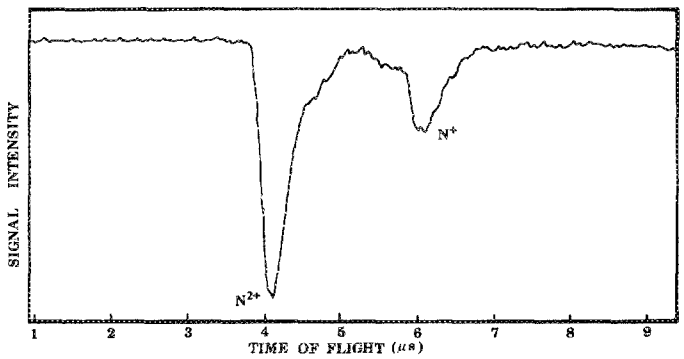


FIG. 9. Time-of-flight ion signal for $N^{2+}$ and $N^{+}$. The trap was set to maximize the storage of $N^{2+}$. The trap contents were sampled by applying a $-70$-V pulse to the end-cap electrode No. 2. The ions were created by electron bombardment of $2\times10^{-7}$ Torr of ultrapure $N_2$.

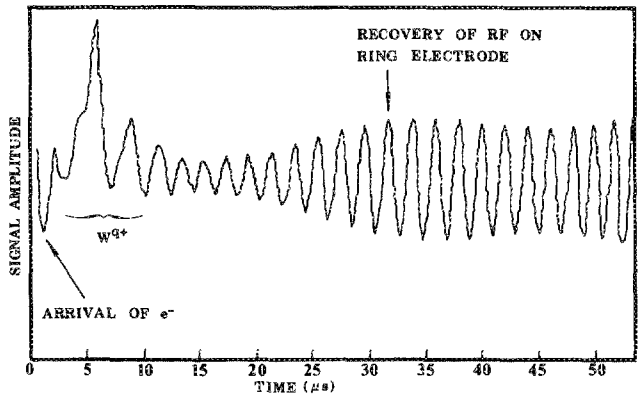


FIG. 10. Langmuir probe signal. The arrival of electrons and ions at the trap is detected almost immediately after ablation, indicating that the mean ion energies must be about 250 eV. The Langmuir probe also picks up rf signal from the ring electrode. The presence for electrons and ions from the laser plasma greatly influence the amplitude and phase of rf at the ring electrode. Notice that during the initial 15 $\mu$s after the ablation, the ring electrode was effectively shorted out. To ascertain that the reduction of rf pickup by the Langmuir probe was not due to shielding of the ring electrode by laser-induced electrons, the rf amplitude at the ring electrode was directly monitored. Their results are consistent.

trajectories of ions in a periodic hyperbolic potential. The charge states of the stored ions are identified by pulsing the ions into a TOF spectrometer previously calibrated with $Ar^{+}$ $(m/q=40)$, $Ar^{2+}$ $(m/q=20)$, $N_2^{+}$ $(m/q=28)$, and $N^{+}$ $(m/q=14)$. Figure 9 gives the TOF spectrum of $N^{2+}$ and $N^{+}$. The mass resolution $(M/dM)$ of this simple TOF spectrometer is about 5, which is quite adequate for the present purpose. The resolution can be improved, should that be warranted by increasing the length of the flight path and the rise time of the dump pulse and/or the terminating resistor for the ion signal. The mass-to-charge identification of the ions is further confirmed by the quadrupole mass analyzer.

### B. Energy measurement of trapped ions

The pseudopotential well depth used for trapping tungsten ions is estimated to be 16 eV for this investigation. The maximum well depth usually gives an upper limit on the energy of the stored ions, and for $W^{2+}$ the value is 0.17 eV/amu. However, the actual energies of these trapped ions must be substantially lower. Figure 10 shows a temporal profile of the laser-induced plasma monitored by the Langmuir probe. Electrons from the ablation plasma first streamed into the ion trap followed by the slower moving heavy ions. The high density of the fast moving electrons temporarily short the ring electrode to ground as indicated by the sharp reduction of rf pickup by the Langmuir probe. The ions moving behind the electrons therefore enter the ion trap without seeing the rf field. The rf recovers its full amplitude only 30 $\mu$s after the arrival of the plasma electron. During this short duration, the trap is unable to store any ion. Ions with energies above $4\times10^{-3}$ eV/amu transverse the full diameter of the trap, while the rf recovers. Ions which are still inside the trap after rf has fully recovered must therefore have energy less than $4\times10^{-3}$ eV/amu.

### C. Storage time of trapped ions

The storage time of the ions in the ion trap is crucial in the charge-transfer measurement. It was determined by monitoring the decrease of the ion-signal magnitude when the stored ions are pulsed out of the trap at progressively longer delay times. A plot of the data obtained is shown in Fig. 11. The characteristic storage time $(1/e)$ is about 85 s for all ions stored. The storage time is limited by charge transfer and elastic collisions between the stored ions and the $10^{-9}$-Torr residual background gas.

### D. Calibration of the ion gauge for absolute pressure measurement

The nude Bayard-Alpert ionization gauge and the Masstorr DX100 and DX200 quadrupole residual gas analyzer used in the vacuum chamber was calibrated using the following procedure. A 1-$\ell$ gas reservoir was connected to the chamber through a leak value. A very thin copper disk with a 1-cm-diam hole in its center was installed to choke the diffusion pump inlet. Assuming molecular flow, the pressure in the vacuum chamber is described by the simple equation[27]

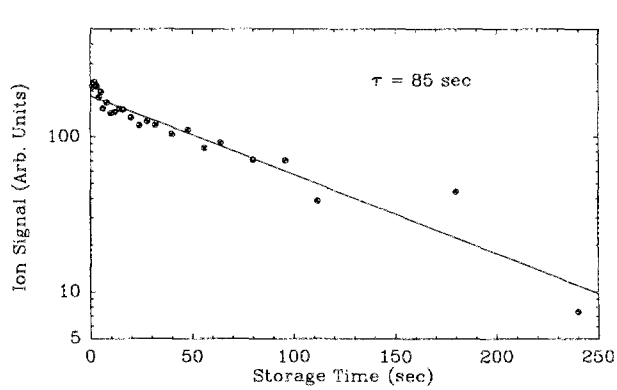


FIG. 11. $W^{4+}$ signal amplitude as a function of storage time. The storage time $(1/e)$ is 85 s.

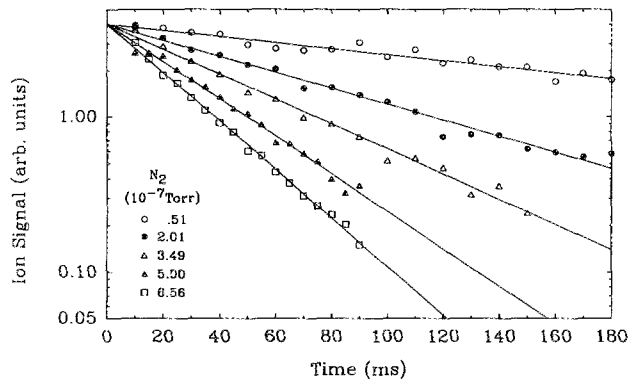


FIG. 12. Decay of $N^{2+}$ vs $N_2$ pressure. Each data point is an average of more than four experimental runs.

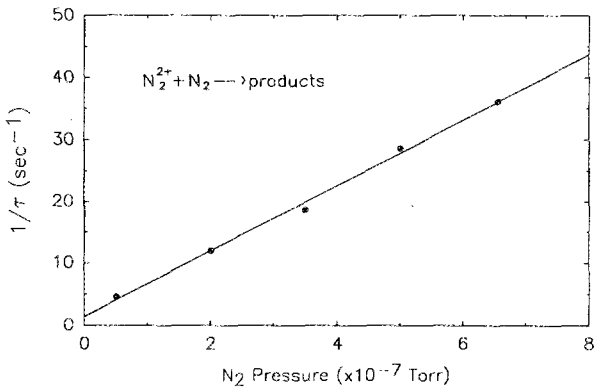


FIG. 13. $N^{2+}$ decay rates as function of $N_2$ gas pressure. The slope is proportional to $\langle Qv \rangle$ for electron capture from $N_2$.

$$P_{\text{chamber}} = P_{\text{reservoir}}(C_{\text{leak value}}/C_{\text{orifice}}) + P_{\text{outgas}},$$

where $P_{\text{reservoir}}$ and $P_{\text{outgas}}$ are the reservoir pressure and pressure due to outgassing; $C_{\text{leak}}$ and $C_{\text{orifice}}$ are the conductances of the leak value and orifice plate, respectively. The conductance of the orifice is calculated for molecular flow from the relation[26]

$$C_{\text{orifice}} = 3.7(T/M)^{1/2}A,$$

where $T$ is the temperature of the gas, $M$ is the molecular weight of the gas, and $A$ is the area of the aperture. The conductance of the leak valve is measured by filling the reservoir with a known amount of gas, setting the leak value to yield a typical vacuum system background pressure, and measuring the reservoir pressure as a function of time. The absolute pressure in the reservoir is measured with a Baratron-type 122A capacitance manometer (accuracy $\pm 0.05\%$). Measurement of the background pressure with no gas load and the pump choked is $1.8\times10^{-8}$ Torr. This base pressure allows us to essentially neglect the outgassing term $P_{\text{outgas}}$ when calibrating the gauges in the $10^{-6}$-Torr region.

### E. Calibration using charge transfer of $N^{2+}+N_2$

The system was tested by measuring the charge-transfer rate of $N^{2+}$ with $N_2$. The vacuum chamber was filled with $N_2$. $N^{2+}$ ($m/q = 7$) was created by electron bombardment of $N_2$. The trapping parameters were chosen to optimize the storage of $N^{2+}$. The $N^{2+}$-ion signal was scanned as a function of delay time after creation. Several measurements were made for each of the six different $N_2$ pressures (see Fig. 12). The charge-transfer coefficient is measured to be $1.73(0.18)\times10^{-9}$ cm$^3$ s$^{-1}$ and is obtained from the slope in Fig. 13. The intercept gives the charge transfer rate of $N^{2+}$ with residual background gas in the vacuum chamber. Their mean rate coefficient is estimated to be $2\times10^{-9}$ cm$^3$ s$^{-1}$.

The charge-transfer coefficient obtained in this measurement compares favorably with earlier result [$K = 2.8(0.6)\times10^{-9}$ cm$^3$ s$^{-1}$] of Church and Holzscheiter.[28] Their result was derived directly from the time constant of $N^{2+}$-ion signal decay. They have assumed that the charge transfer between $N_2$ and $N^{2+}$ is the dominant process that removed $N^{2+}$ from their Penning trap.

### F. Measurement of $W^{2+}+Ar$

$W^{2+}$ was generated and trapped using the colliding laser ablation beams. The ion-signal data are fitted with a single exponential decay curve. The characteristic decay times for six argon pressure runs are plotted as a function of argon pressure (see Fig. 14). An uncertainty weighted least-squares fit to those six points gives a rate coefficient for the charge transfer between Ar and $W^{2+}$ of $0.99(0.22)\times10^{-11}$ cm$^3$ s$^{-1}$. The estimated uncertainty of the result is $\pm 22\%$ and is mainly due to the uncertainty in the statistical fluctuation of the ion signals.

## ACKNOWLEDGMENTS

We thank W. H. Parkinson and Alex Dalgarno for their suggestions and encouragement, and J. C. Selser and David Emerson for their support in various phases of this work. We also acknowledge the technical assistance of Chun Zhang, Barbara Stevenson, and Judy Earl. This work is supported in part by Grant No. RII-8410674 from

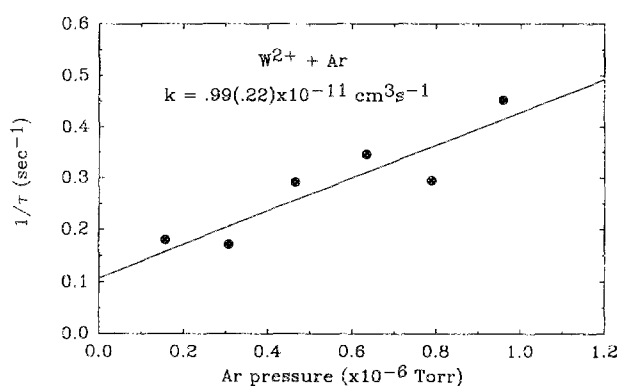


FIG. 14. $W^{2+}$ decay rates as function of Ar pressure. Slope is proportional to $\langle Qv \rangle$ for electron capture from Ar. Intercept at zero Ar pressure gives the $\langle Qv \rangle$ for electron capture from residual background gas ($H_2O$, $H_2$) in the vacuum system.

the National Science Foundation (EPSCoR) to the University of Nevada System, the Joseph H. deFrees Grant of the Research Corporation, and a grant from the UNLV Research Council.

[1] D. R. Bates and B. L. Moiseiwitsch, Proc. Phys. Soc. (London) A **67**, 805 (1954).
[2] S. E. Butler, T. G. Heil, and A. Dalgarno, Ap. J. **241**, 442 (1980).
[3] R. B. Christensen, W. D. Watson, and R. J. Blint, Ap. J. **213**, 712 (1977).
[4] D. E. Post, in *Physics of Ion–Ion and Electron–Ion Collision*, edited by R. Brouillard and J. W. McGowan (Plenum, New York, 1983), p. 60.
[5] R. K. Janev, J. Phys. (Paris) Colloq. **50**, C1-421 (1989).
[6] C. F. Melius, J. Phys. B **7**, 1692 (1974).
[7] R. J. Dewhurst, D. Jacoby, G. J. Pert, and S. A. Ramsden, Phys. Rev. Lett. **37**, 1265 (1976).
[8] W. H. Louisell and M. O. Scully, Phys. Rev. A **11**, 989 (1975).
[9] R. H. Dixon, J. F. Seeley, and R. C. Elton, Phys. Rev. Lett. **40**, 122 (1978).
[10] L. D. Gardner, H. E. Bayfield, P. M. Koch, I. A. Sellin, D. J. Pegg, R. S. Peterson, R. S. Mallory, M. L. Mallory, and D. H. Crandall, Phys. Rev. A **20**, 766 (1979).
[11] T. Iwai, Y. Kaneko, M. Kimura, N. Kobayashi, S. Ohtani, K. Okuno, S. Takagi, H. Tawava, and S. Tsurubuchi, Phys. Rev. A **26**, 105 (1982).
[12] R. W. McCullough, T. V. Goffe, M. B. Shan, M. Lennon, and H. B. Gilbody, J. Phys. B **15**, 111 (1982).
[13] D. A. Church and H. M. Holzscheiter, Phys. Rev. Lett. **49**, 643 (1982).
[14] C. R. Vane, M. H. Prior, and R. Marrus, Phys. Rev. Lett. **46**, 107 (1981).
[15] C. C. Havener, M. S. Huq, H. F. Krause, P. A. Schulz, and R. A. Phaneuf, Phys. Rev. A **39**, 1725 (1989).
[16] H. F. Winters and Inokuti, Phys. Rev. A **25**, 1420 (1982).
[17] R. D. Knight, Appl. Phys. Lett. **38**, 221 (1981).
[18] D. A. Church, S. D. Kravis, I. A. Sellin, C. S. O., J. C. Levin, R. T. Short, M. Meron, B. M. Johnson, and K. W. Jones, Phys. Rev. A **36**, 2487 (1987).
[19] M. A. Levine, R. E. Marrs, J. R. Henderson, D. A. Knapp, and M. B. Schneider, Phy. Scr. T **22**, 157 (1988).
[20] R. E. Marrs, M. A. Levine, D. A. Knapp, and J. R. Henderson, Phys. Rev. Lett. **60**, 1715 (1988).
[21] V. H. S. Kwong, Phys. Rev. A **39**, 4451 (1989).
[22] R. M. Measures, N. Drewell, and H. S. Kwong, Phys. Rev. A **16**, 1093 (1977).
[23] A. W. Ehler, Appl. Phys. **37**, 4962 (1966).
[24] F. E. Irons, R. W. O. McWhirter, and N. J. Peacock, J. Phys. B **5**, 1975 (1972).
[25] R. A. Phaneuf, Phys. Rev. A **24**, 1138 (1981).
[26] E. Jahnke, F. Emde, and F. Losch, *Table of Higher Function* (Verlagsgesellschaft, Stuttgart, 1960).
[27] J. F. O'Hanlon, *A User's Guide to Vacuum Technology* (Wiley, New York, 1980).
[28] D. A. Church and H. M. Holzscheiter, Chem. Phys. Lett. **76**, 109 (1980).